A staggered compact WENO scheme for the scalar transport equations used with the compressible Navier-Stokes equations.

Pratik Nayak[1], Bendiks Jan Boersma[2]

Laboratory for Process and Energy, Mekelweg 2, 2628 CD Delft, The Netherlands

Abstract

In this paper, compact schemes with non-oscillatory properties are developed which derive their stability and high spatial resolution properties from the staggered compact finite difference schemes of Boersma [1] and the low dissipation, hybrid non-oscillatory properties from [2]. This method has been applied specifically to the case of the compressible turbulent jet to demonstrate its applicability to the passive scalar transport which requires the non-oscillatory property for a physically correct solution. The results and the test cases show that the method is suitable for such flows and can be easily applied to study physical processes such as combustion.

Keywords: Direct Numerical Simulation, compact WENO, Turbulence

1. Introduction

Direct Numerical Simulations (DNS) are the class of methods in Computational Fluid Dynamics(CFD) that strive to simulate the flow without any modelling for the effects of turbulence. Therefore, these methods have to capture a wide range of scales. Hence their applicability has been limited by computational power. A detailed review of DNS and its usage has been given by Mahesh et.al. [3].

[1] p.v.nayak@student.tudelft.nl
[2] B.J.Boersma@tudelft.nl

High order methods such as the compact finite difference methods have been widely used for DNS and LES methods for studying flows due to their capability to have a very good resolution which is essential in DNS. Several variants of the compact finite methods have been proposed. Lele [4] first used these methods because they had spectral like resolution with better stability properties. Mahesh [5] then proposed methods which calculated both the first and second derivatives and thereby using less computational power. Boersma [1] proposed compact finite difference methods on a staggered grid which had better stability properties than those of [4] and [5]. These methods have been shown to be widely applicable [6], [7], [8], [9] and even in fields such as finance [10].

In simulations of compressible flows at high Mach (close to one) and Reynolds numbers, these compact difference methods are advantageous because they have low dissipation due to the central nature but also face problems such as oscillations near the discontinuities [1]. For certain problems these oscillations can make the solution unphysical. For example, the concentration of reactants in a reactive flow can become negative which is not physical. Therefore for equations such as the scalar transport equation a non-oscillatory method (such as WENO) needs to be used to ensure the correctness of the solution.

Different authors have observed that when these hyperbolic pde's with large characteristic speeds are modeled using central methods (methods taking information from both sides of the discontinuity), oscillations are observed which can make the solution unphysical [1]. Therefore, to remove these oscillations a different class of methods must be used. The class of methods that have been used in this paper are called the WENO methods, Weighted Essentially Non-Oscillatory methods. They are an improvement of the ENO (Essentially Non-Oscillatory) methods first introduced by Harten et.al [11]. The idea was to consider many candidate stencils rather than one stencil and measure "smoothness" of the function in the stencils and choose the stencil in which the function is the "smoothest" in some sense. These class of methods were very effective for problems that contained discontinuities but were dissipative. This made the methods quite popular even though the methods are sometimes disspative. Var-

ious researchers worked to improve the ENO methods to improve the measuring of smoothness, choosing of stencils and to reduce the dissipation. [12, 13, 14]. It was recognized by Liu, Osher and Chan [15] that instead of choosing a smoothest stencil, one could choose a convex combination of all the stencils thereby giving a weight to each of the stencils depending on the smoothness of the function in the respective stencils. These methods were called the WENO methods. Jiang and Shu [16] did an extensive study of the methods and developed a new method to estimate the smoothness indicators which was more efficient and robust than the divided difference methods used in the previous ENO methods. This smoothness indicator was based on the measurement of the total variation of the function in the stencil and are extensively used in almost all WENO and WENO derived methods today. An added advantage of the WENO methods was that the convex combination of the stencils increased the accuracy in the smooth regions as explained in [16] while capturing discontinuities and reverting to the normal order in the regions of discontinuities. This was not possible in ENO because only a single stencil was chosen and hence the maximum order even in the smooth regions was limited.

With WENO, many improvements were still possible. The numerical dispersion was still quite high enough that the resolution of short waves was not good enough. Tam and Webb [17] developed dispersion relation preserving schemes that were suitable for aero-acoustics simulations where even the capture of small disturbances was important. Martin et.al [18] developed schemes that were optimal based on the bandwidth and suitable for compressible turbulent flows. Another aspect of the WENO schemes were that they were still quite dissipative. Due to the inherent upwinding to capture the discontinuities, a lot of numerical dissipation was introduced in the schemes. This numerical dissipation is not desirable for flows that have to resolve a wide range of of scales and especially flows where the high wavenumbers play an important role. In general, dissipation can be reduced by two methods, one being the usage of a hybrid scheme, that is schemes that used sub-schemes that had lesser dissipation in the smooth regions. Adams and Sharif [19] used a hybrid version of

the compact upwind and the ENO schemes as a start to these hybrid methods. Ren et.al [20] considered schemes that were a hybrid of the WENO and the compact schemes and improved the transition between the sub-schemes. The other idea was to use central symmetrical stencils. This was pursued by Martin et.al [18], but the solution degenerated near critical points. Another idea was to map the non-linear WENO weights so that they would have a lesser dissipation and better properties. This was introduced by Henrick et. al [21] They mapped the traditional WENO schemes and obtained better properties. Finally, Liu et al.[2] pursued schemes that were a hybrid of the central compact and the WENO schemes. They used grid points on both staggered and co-located grids to calculate the derivatives of the fields. Their weighting procedure involved the usage of lower order upwind stencils as well as high order central stencils and the calculation of smoothness of the fields in these stencils to obtain, first linear weights and then non-linear weights which then formed the overall scheme. The weights, both non-linear and linear were dependent on user defined constants which are to be set based on the nature of the problem.

This paper aims to combine the aspects of stability even at a low resolution from the staggered compact finite difference methods [1] and the WENO methods which are essential in certain flows to make these methods suitable for DNS and LES by adding an additional hybrid compact WENO interpolation to the scalar transport equation with a Lagrangian approach for the boundary conditions. These non-oscillatory methods are essential to accurately capture the physics in certain flows such as the ones that involve combustion or chemical reactions.

The paper is organized as follows. Section 2 gives the governing equations used for the physically relevant test case. Section 3 explains the computational methods used, Section 4 explains the implementation approach, Section 5 aims to validate the method with two simple tests and a test case from a physical problem of the compressible turbulent jet and the paper finally concludes with Section 6.

2. Governing Equations

The governing equations involved are the conservation of mass, momentum, energy and the ideal gas equation to close the set of equations. Additionally, the scalar transport equation is also solved for the transport of a passive scalar. The conservation of mass is written as

$$\partial_t \rho + \partial_i(\rho u_j) = 0 \tag{1}$$

where ρ is the fluid density, u_j is the velocity vector. The conservation of momentum equation can be written as

$$\partial_t(\rho u_i) + \partial_j(\rho u_i u_j + p\delta_{ij}) = \partial_j \tau_{ij} \tag{2}$$

where p is the pressure and τ_{ij} is the viscous stress tensor. As only Newtonian fluids are considered here, the viscous stress tensor is defined as

$$\tau_{ij} = \mu\{\partial_j u_i + \partial_i u_j - 2(\partial_k u_k)/3\} \tag{3}$$

where μ is the dynamic viscosity of the fluid. In this paper, the dynamic viscosity is not constant but dependent on the temperature through the Sutherland relation [22]

$$\mu/\mu_\infty = (T/T_\infty)^{3/2}(1.4T_\infty)/(T + 0.4T_\infty) \tag{4}$$

where μ_∞ and T_∞ are the ambient values. The conservation of energy equation can be written as

$$\partial_t E + \partial_j(u_j(p + E)) = \partial_j(\kappa(\partial_j T)) + \partial_j(u_i \tau_{ij}) \tag{5}$$

where E is the total energy and is the sum of internal energy, $e = \rho c_v T$ and kinetic energy, $K = \rho u_i u_i/2$ that is $E = e + K$. κ denotes the thermal conductivity given by $\kappa = \mu c_p/Pr$. c_p is the specific heat at constant pressure and Pr is the Prandtl number which denotes the ratio of the momentum to the thermal diffusivity. c_p is given based on the properties of the gas. The equation of state for an ideal gas gives the relation between the thermodynamic quantities, ρ, p and T as

$$p = \rho R T \tag{6}$$

where R is the gas constant. Subsequently, the speed of sound is given by, $c_\infty = U_{sound} = \sqrt{\gamma RT}$, where γ is the ratio of specific heats, $\gamma = c_p/c_v$.

All the variables are non-dimensionalized using the ambient speed of sound, c_∞, the ambient density ρ_∞, the ambient pressure $\rho_\infty c_\infty^2$, the ambient temperature, c_∞^2/c_p and the ambient concentration, $Y_{k,\infty}$ as the reference scales to obtain the non-dimensional numbers Reynolds, Mach, Prandtl and Schmidt numbers to govern the physics of the flow whose values used in the experiments are given in Section 5.3.

The scalar transport equation which governs the distribution of the passive scalar in the flow can be written as

$$\partial_t(\rho Y_k) + \partial_j(\rho u_j Y_k) = -\partial_j(\rho \kappa_{scal}(\partial_j Y_k)) + \omega_k \tag{7}$$

where Y_k is the concentration of the kth chemical species where $k \in \{1, 2, ..., n\}$ and ω_k is the chemical source term which can form the source or sink for the kth chemical species $\boldsymbol{j}_k$ is the diffusive flux which is approximated by a binary flux approximation [23, 24, 25]. One has to be careful when using multi-component species as, with a binary flux approximation, the mass conservation for the all species may not be satisfied and a different flux approximation may have to be used. But for the purposes of this paper, a binary flux approximation will be used and is given by $\boldsymbol{j}_k = -\rho \kappa_{scal} \nabla Y_k$.

3. Computational Methods

This section is divided into three parts, the spatial discretization, the temporal discretization and the parallel implementation.

3.1. Spatial discretization

The main method of spatial discretization for the mass, momentum and the energy equation is the staggered compact finite difference method of Boersma which has been explained in detail in [1]. This paper is concerned with the discretization of the scalar transport equation which is essentially an advection diffusion equation with a possible source term. To capture the accurate

physics, an additional WENO interpolation is done which makes the solution non-oscillatory.

The spatial derivative is calculated using the compact finite difference method of Boersma [1] which is given as

$$\alpha f'_{i-1} + f'_i + \alpha f'_{i+1} = d\frac{f_{i+7/2} - f_{i-7/2}}{h} + c\frac{f_{i+5/2} - f_{i-5/2}}{h} + b\frac{f_{i+3/2} - f_{i-3/2}}{h} + a\frac{f_{i+1/2} - f_{i-1/2}}{h} \tag{8}$$

where a prime denotes the derivative of the function f. Only a formula for a first derivative is required unlike in [5] where both derivatives are calculated at once because the conservative form of the equation is solved for and the second derivative is calculated as the derivative of the first derivative. The coefficients are matched as done in [1] and in [4] with the corresponding Taylor series expansions. As the grid used was a staggered grid as shown in Figure 1

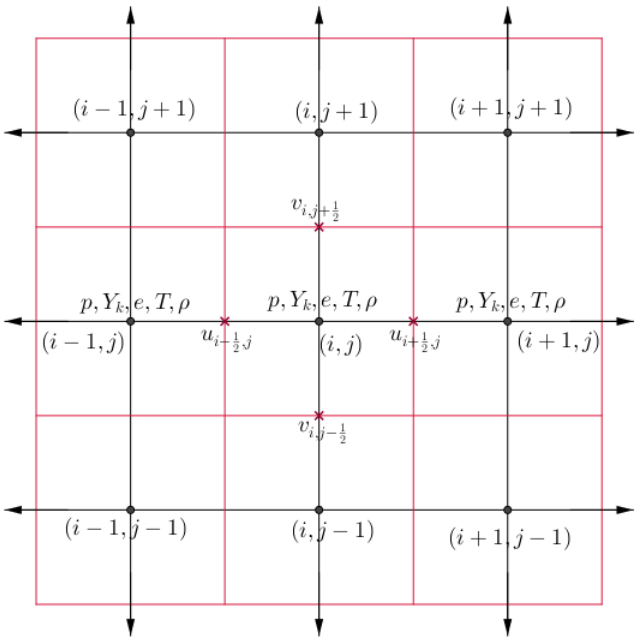

Figure 1: 2D grid for discretization

The velocities, u, v, w are on the cell faces and the scalars are on the cell centers. When a product is to be calculated, such as the mass flux, ρu, then

both the quantities must be multiplied when at the same point. Therefore, an interpolation formula is needed which is also a compact interpolation formula given as

$$\begin{aligned}\hat{\alpha}f_{i-1} + f_i + \hat{\alpha}f_{i+1} = \hat{d}(f_{i+7/2} + f_{i-7/2}) + \hat{c}(f_{i+5/2} + f_{i-5/2}) \\ +\hat{b}(f_{i+3/2} + f_{i-3/2}) + \hat{a}(f_{i+1/2} + f_{i-1/2})\end{aligned} \tag{9}$$

The coefficients are given in [1] The WENO interpolation follows the same idea as in the paper of Liu [2], which is a hybrid compact scheme. The main idea of WENO is to use multiple stencils and measure the smoothness of the required function in the stencils and take a convex combination of the stencils. This allows for a higher order while producing a non-oscillatory solution.

The WENO idea in [26], was to interpolate the value of the function f at the cell center, $x_{i+\frac{1}{2}}$ by a $(2r-1)$ order approximation by

$$\tilde{f}_{i+\frac{1}{2}} = g^{2r-1}(f_{i-r+1}, ..., f_{i+r-1}) \tag{10}$$

The stencil, S^{2r-1} is split into r sub-stencils from $k = 0, ..., (2r-1)$ as

$$S_k^{2r-1} = (x_{i+k-r+1}, ..., x_{i+k}) \tag{11}$$

and using the r-th order approximation from each of the stencils,

$$\tilde{f}^k_{i+\frac{1}{2}} = g^r_k(f_{i+k-r+1}, ..., f_{i+k}) \tag{12}$$

where

$$g^r_k(w_0, ..., w_{r-1}) = \sum_{j=0}^{r-1} a^r_{kj} w_j \tag{13}$$

to form a convex combination of the interpolations above to get

$$\tilde{f}_{i+\frac{1}{2}} = \sum_{k=0}^{r-1} \omega^r_k g^r_k(f_{i+k-r+1}, ..., f_{i+k}) \tag{14}$$

where ω^r_k is the non-linear weights dependent on the smoothness in each of the stencils.

To combine with the compact finite difference method, we just substitute the interpolated values to Equation 8 to get the derivative of the required function.

As discussed before, central schemes have very low dissipation and upwind schemes have high dissipation. Dissipation is required to capture discontinuities and hence the WENO scheme uses the upwind stencil to accurately model the discontinuities. An idea proposed by Liu et al [2] proposes a hybrid weighted non-linear interpolation that incorporates the idea of WENO to assign weights to a hybrid scheme consisting of upwind and central stencils. A hybrid linear interpolation can be written as

$$\tilde{f}^{hyb}_{i+\frac{1}{2}} = (1-\sigma)\tilde{f}^{upw}_{i+\frac{1}{2}} + \sigma\tilde{f}^{cent}_{i+\frac{1}{2}} = \sum_{j=0}^{3} y_j \tilde{f}^{j}_{i+\frac{1}{2}} \tag{15}$$

where y_j are the linear weights and σ is the parameter that controls the contribution of the upwind and the central stencil and $0 \leq \sigma \leq 1$. As seen, if $\sigma = 1$, then it is a fully central scheme and if $\sigma = 0$, then it is a upwind scheme with no central contribution. For the definition of σ we use the ideas from Ren et. al. [20]. They suggests a σ to be defined as a continuous function rather than a abrupt function as done by Pirozzoli [27] and defines it as

$$\sigma = min\left(1, \frac{\varrho_{i+\frac{1}{2}}}{\varrho_c}\right) \tag{16}$$

where ϱ_c is a parameter that controls the dissipation and $\varrho_{i+\frac{1}{2}}$ is a smoothness indicator defined by $\varrho_{i+\frac{1}{2}} = min(\varrho_{i-1}, \varrho_i, \varrho_{i+1}, \varrho_{i+2})$ and ϱ_i has been defined by

$$\varrho_i = \frac{|2(f_{i+1} - f_i)(f_i - f_{i-1})| + \delta}{(f_{i+1} - f_i)^2 + (f_i - f_{i-1})^2 + \delta} \tag{17}$$

where δ is another parameter that gains importance for DNS of turbulent, viscous flows, because of the turbulent fluctuations which may make the smoothness indicator very small making the scheme very dissipative when WENO is used. Hence to reduce the dissipation and to make sure that the turbulent fluctuations are not damped, Ren et. al. [20] suggests to use δ as

$$\delta = \frac{0.9\varrho_c}{1 - 0.9\varrho_c}\xi^2 \tag{18}$$

and ξ is a parameter that controls the dissipation and it has been verified that when $max((f_i - f_{i-1}), (f_{i+1} - f_i), (f_{i+2} - f_{i+1})) \leq \xi$, we get $\sigma \geq 0.9$, therefore

making the central sub-scheme dominate the hybrid scheme. The value of ξ serves as a threshold value and turbulent fluctuations lesser than ξ will not be damped by the WENO scheme. Writing it explicitly we obtain the final form for an example for the 6th order compact WENO as in [2], we get

$$\begin{aligned}\tilde{f}^{hyb,lin}_{i+\frac{1}{2}} &= \frac{3y_0}{8}f_{i-2} - \frac{10y_0+y_1}{8}f_{i-1} \\ &+ \frac{15y_0+6y_1+3y_2}{8}f_i + \frac{3y_1+6y_2+15y_3}{8}f_{i+1} \\ &- \frac{y_2+10y_3}{8}f_{i+2} + \frac{3y_3}{8}f_{i+3}\end{aligned} \tag{19}$$

The linear weights are given by

$$y_0 = \frac{2-\sigma}{32}, y_1 = \frac{5(4-\sigma)}{32}, y_2 = \frac{5(2+\sigma)}{32}, y_3 = \frac{\sigma}{32} \tag{20}$$

To get the WENO scheme, we replace the linear weights by the non-linear weights. Therefore, the hybrid non-linear interpolation is

$$\begin{aligned}\tilde{f}^{hyb}_{i+\frac{1}{2}} &= \frac{3\omega_0}{8}f_{i-2} - \frac{10\omega_0+\omega_1}{8}f_{i-1} \\ &+ \frac{15\omega_0+6\omega_1+3\omega_2}{8}f_i + \frac{3\omega_1+6\omega_2+15\omega_3}{8}f_{i+1} \\ &- \frac{\omega_2+10\omega_3}{8}f_{i+2} + \frac{3\omega_3}{8}f_{i+3}\end{aligned} \tag{21}$$

where the non-linear weights, ω_j are the WENO weights given by

$$\omega_j = \frac{\alpha_j}{\sum_{d=0}^{3}\alpha_d}, \qquad \alpha_j = y_j\left(C + \frac{\tau}{\epsilon+\beta_j}\right), \qquad j = 0, ..., 3 \tag{22}$$

where the α_j above is defined to include both the linear weights and the non-linear weights and hence is different from the usual WENO weights. C is a parameter that assigns a weight to the linear part of the weight. As observed by Hu [28], changing C changes the numerical dissipation only slightly. A larger C produces less numerical dissipation. Very large values of C produce numerical instabilities for flows with strong shocks. ϵ is a small positive number of order machine precision used to prevent the denominator from going to zero. τ is called the reference smoothness indicator defined by

$$\tau = \beta_3 - \frac{1}{8}(\beta_0 + 6\beta_1 + \beta_2) \tag{23}$$

and finally the smoothness indicators, β_j are as given in [2].

When an upwind scheme is used, the characteristic velocity of the equation must be looked at carefully. Depending on whether the derivative of the flux is positive or negative, the scheme would be upwind or downwind and therefore the stencil must be adapted accordingly. All the above interpolations are given for a positive flux derivative. When the flux derivative is negative, the stencil is mirrored about the point $x_{i+\frac{1}{2}}$. It is important to split the fluxes appropriately to make sure that the upwind stencil is only used on the positive fluxes and the downwind on the negative fluxes.

In general, it is possible to split the fluxes into positive and negative fluxes. The important aspect to note while splitting the fluxes is that we need to have the split fluxes to have as many derivative as the order of the scheme in the least. There are many choices for flux splitting methods.

We use the Lax-Friedrichs flux splitting, where the total flux is split as $f^{\pm}(u) = \frac{1}{2}(f(u) \pm \alpha u)$. There are two variants of the Lax-Friedrichs splitting, one is the global splitting and the other is the local splitting, the difference between the two being the value of $\alpha = \max(|f'(u)|)$, where the maximum is taken over either the global or the local range of u. For the advection equation, the $f'(u)$ is nothing but the Jacobian of the governing equation and sometimes called the characteristic velocity which is also the slope of the characteristics of the solution when using the method of characteristics.

3.2. Temporal Discretization

As the flow to be studied here is a turbulent, unsteady flow, we use explicit methods. The most well known explicit methods are the Runge Kutta family of methods. The Runge-Kutta 4th order method has been used in this paper as in Table 1.

For a detailed analysis of the stability analysis of the Runge-Kutta methods using Fourier analysis and stability plots that define the time step restrictions based on the CFL number, one can refer [29, 30].

Table 1: Butcher Tableau - RK4

0				
$\frac{1}{2}$	$\frac{1}{2}$			
$\frac{1}{2}$	0	$\frac{1}{2}$		
1	0	0	1	
	$\frac{1}{6}$	$\frac{1}{3}$	$\frac{1}{3}$	$\frac{1}{6}$

3.3. Boundary conditions

Apart from the usual boundary conditions, for numerical implementations, numerical boundary conditions (compatibility relations) are sometimes required to solve for unknowns not specified at the boundaries. As we work in a Cartesian grid, our domain is a box and hence we have six face boundaries. The left boundary along the x axis is the inflow boundary where the jet enters the domain through the nozzle as shown in Figure 2. The domain starts at the exit of the nozzle and the nozzle is not a part of the domain. The right boundary along x is the outflow boundary. The four other faces form the walls and have normals that are perpendicular to the x direction.

This paper makes use of the ambient boundary conditions in which the quantities at the boundaries are set to the far-field ambient values. This means that for the boundary condition to make sense and be physical, one has to either increase the domain size to allow for the physical region of influence of the jet to be far from the boundaries emulating the far-field region or one can use sponge layers and damping methods to reduce the abrupt change of the quantities when the boundaries are close to the physical region of influence of the jet.

In general the well known boundary conditions are as developed by Poinsot et.al. [31] and Thompson [32]. But these boundary conditions require a large domain when ambient conditions are used as they may produce reflections which can influence the solution. In this paper, the basic idea of the boundary con-

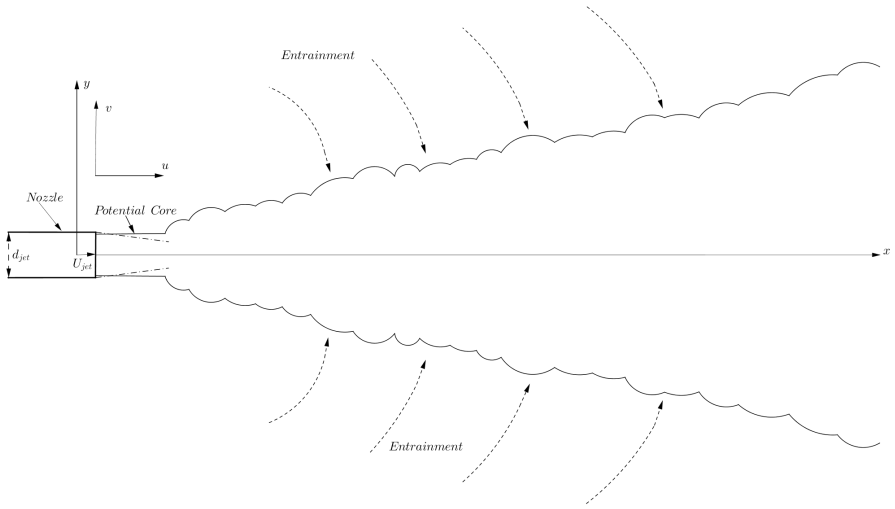

Figure 2: The free turbulent jet geometry

ditions being the same as Poinsot et.al. [31], additional damping layers were added to ensure that the solution was reflection free.

As given in [31], for a subsonic inlet, the boundary conditions are not well defined. Therefore, an artificial convection velocity is added to the axial velocity to make it locally supersonic. This is also done at the outflow where the flow is convected out of the domain axially with an additional axial velocity. This supersonic velocity at the inflow and the outflow means that the no other flow variables need to be specified at the outflow to obtain a well-defined problem. The artificial convection velocity is reduced to zero uniformly in the interior of the domain. The region where the artificial convection velocity is added is limited to a region very close to the inflow and the outflow of the domain so that the solution is not affected by it. At the boundaries whose normals are perpendicular to the axial direction, the flow variables are set to ambient conditions. Even though this is strictly not true, but due to computational and physical constraints to limit the domains, we impose this. As these boundaries

are far away (effectively, due to the damping and sponge layers) from the region of influence of the jet, this condition still gives meaningful results. Additionally, damping layers are added to ensure that the reflection from the boundaries do not affect the solution.

4. Implementation

The first aspect of parallelization is the decomposition of the domain and assignment of the different processes to the sub-divided domains. The code in this paper uses the `2decomp` [3] pencil decomposition library to divide the domain. As the problem in consideration is a three-dimensional problem, the x, y and z directional solutions are done sequentially. The x and the z solves are done with in one logical arrangement. The data is then transposed such that there are no divisions perpendicular to the y axis and the y solves are done with this logical arrangement.

This paper uses the staggered schemes of Boersma [1] to differentiate each of the terms and to interpolate between the staggered and the co-located grids when needed. The scalars, ρ, e, T, Y_k are present on the cell centers whereas the vector fields, u, v, w are on the cell faces corresponding to the respective normal directions.

4.1. Conservation of mass

The mass conservation equation is given in Equation 1. This equation requires the spatial derivative of the mass fluxes, ρu_j with respect to the direction x_j. First the density is interpolated to the face in the direction of x_j, and multiplied with u_j to form the flux product. This is stored for further use. The term $\partial(\rho u_j)/\partial x_j$ is then calculated at the cell center. The equation is then stepped in time.

[3] 2decomp:http://www.2decomp.org/index.html

4.2. Conservation of momentum

The momentum equations are given in Equation 2. They are a set of three equations in the x, y, z directions. Two terms can be identified here: the convective terms, $\partial(\rho u_j u_i)/\partial x_j$ and the diffusive terms, $\partial(\tau_{ij})/\partial x_j$. For the convective term, $\partial(\rho u_j u_j)/\partial x_j$, the velocities, u_j's are interpolated to the cell centers and the derivative is computed at the cell faces. For the term $\partial(\rho u_j u_i)/\partial x_j$, the flux, ρu_j and velocity u_i are interpolated to the cell corner and the derivative is obtained at the cell face. The pressure gradient for the x momentum equation is calculated at the cell face directly as the values are already available at the cell centers. The diffusive terms are also calculated in a similar fashion where the role of the flux is taken by the first derivative. The terms are added and the equation is stepped in time to obtain the fluxes through which the velocities are then reconstructed.

4.3. Conservation of energy and scalars

Both the scalar conservation equations have two main terms, the convective terms and the diffusive terms. The convective terms, $\partial((E + p)u_j)/\partial x_j$ and $\partial(Y_k \rho u_j)/\partial x_j$ are calculated by interpolating the scalars, E, Y_k to the cell faces and multiplying with the velocities and calculating the derivative at the cell centers. The diffusive terms involve the calculation of a first derivative term of the scalar (T or Y_k), which is calculated at cell face directly and multiplication of that with the diffusion coefficients, κ which is interpolated to the cell face and multiplied with the derivative previously calculated and the final derivative is calculated at the cell center. The last term for the energy equation includes a derivative term that models the energy diffusion by shear. The shear stress term, τ_{ij} is interpolated to the cell face and multiplied with the velocity, u_j and stored during the solution of the momentum equation. This term is then used here and the final derivative is calculated at the cell center.

For the scalar equation, the WENO method has been used to remove the oscillations that were occurring if solved without a non-oscillatory method. The WENO interpolation is required only for the convective terms in the scalar

equation and before taking the derivative, the terms are interpolated through a WENO procedure. Therefore, for the convective terms of the form $\partial(Y_k \rho u_j)/\partial x_j$, the velocity, u_j is interpolated to the cell center and the product $Y_k \rho u_j$ is formed. This quantity is then interpolated using the WENO procedure as in Equation 21 to the cell faces and the derivative is calculated. As this is a convective term and the WENO interpolation involves stencils some of which are upwind(downwind) and that the convective velocity (ρu_j) can be positive or negative, we need to use a flux splitting method to use the appropriate stencils. A Lax-Friedrichs flux splitting was used. The convective velocity was the interpolated velocity (to the cell center) multiplied with the density. After the WENO interpolation the derivative of the term was taken using the compact finite difference method of Boersma [1].

The stencils for the WENO interpolations are centered about $x_{i+1/2}$. This means that at the left and right boundaries in all the three spatial directions, appropriate ghost values need to be calculated. This is done using a simple Lagrangian extrapolation procedure. This procedure is similar to the Lax-Wendroff procedure[33] which is a more generalized version of the Lagrangian extrapolation procedure.

5. Numerical Tests

This section compares the different methods and shows the improvement possible due to the WENO methods. Two test cases were considered, the advection equation and a solid body rotation which is equivalent to a 2D advection case which has been taken from the paper of Zalesak [34].

5.1. The Advection equation

The advection equation as shown in Equation 24 is an important test case for all numerical methods as the exact solution is known and the behaviour is very well understood. Even though it is a simple linear equation, for some initial

conditions, it can be difficult to accurately solve the equation.

$$(C_{test})_t + u_{test}(C_{test})_x = 0 \tag{24}$$

Two initial conditions were considered. One being a smooth initial condition, a sine wave and another being a square wave, with two sharp discontinuities. For both cases, the advection velocity, $u_{test} = 1.0$. The final time, $t_{end} = 10.0$. The number of grid points was equal to 100 for the square wave and 50 for the sine wave. The CFL number, CFL $= \frac{dt|u_{test}|}{dx}$ was set at 0.7. To emulate the effects of interpolation between the cell centers and cell faces in the problem, the values of C_{test} originally at the cell centers were interpolated to the cell faces. For just the compact finite differencing method, the derivative at the cell faces were taken to obtain the values of the derivatives at the cell centers. For the compact WENO methods, the cell face values were interpolated back to the cell centers and the final derivative was taken using the values from the cell centers and the cell faces as done by Liu et al. [2].

Figure 3 shows the comparison between the two schemes for the solution of the advection equation. The following observations can be made:

1. The compact finite difference scheme oscillates near the discontinuities which makes it unsuitable for problems with strong discontinuities, Figures 3(a),3(b). For a smooth initial condition, it behaves very well as can be seen from Figures 3(c),3(d).
2. The WENO 4^{th} order scheme does not oscillate either with the smooth initial condition or in the presence of strong discontinuities.

From the above test, we showed the need for the WENO methods and the situation in which WENO methods are required. As the computational effort required by the 4^{th} order interpolation is lesser than that of the 6^{th} order interpolation and that the 4^{th} order interpolation is stable and non-oscillatory, this paper demostrates the 4^{th} order interpolation for all simulations but alternatively the 6^{th} order could be used as well.

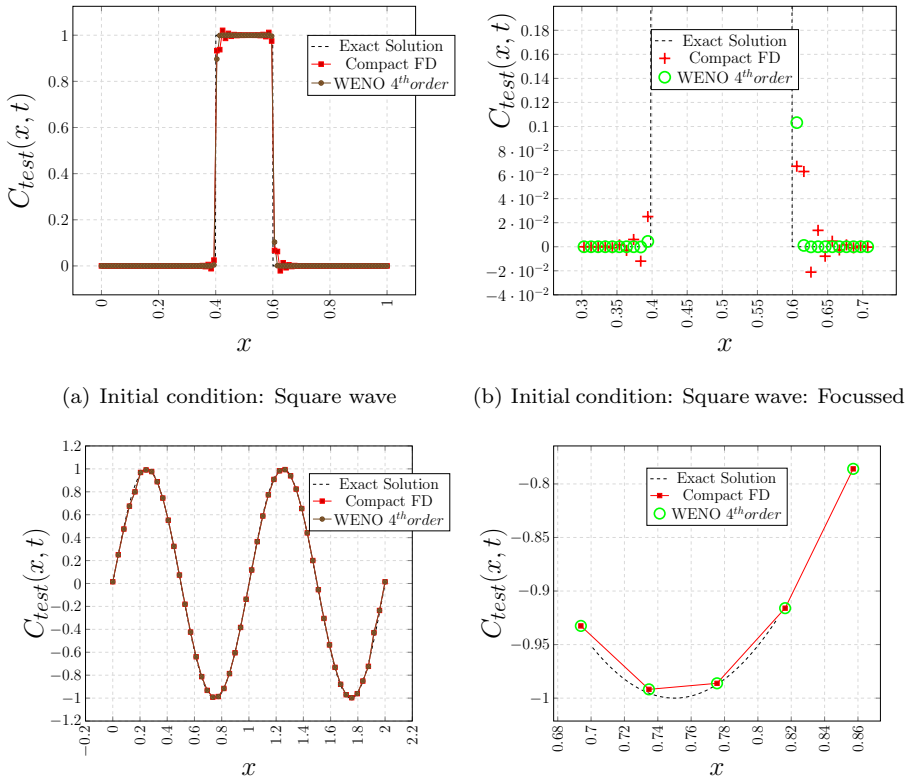

(a) Initial condition: Square wave

(b) Initial condition: Square wave: Focussed

(c) Initial condition: Sine wave

(d) Initial condition: Sine wave: Focussed

Figure 3: Numerical Tests: Comparison of WENO with central compact schemes

5.2. Slotted disk test

The slotted disk test as shown in Equation 25 is a test case that demonstrates the effectivity of the method in 2D. Though, it is very difficult to find a physical application where no diffusion is involved, this method shows the effectiveness of the method where the oscillations are reduced and the numerical dissipation added is also minimal.

$$\begin{aligned} (C_{test})_t + f_x + g_y &= 0 \\ f &= -\Omega(y - y_0)C_{test} \\ g &= \Omega(x - x_0)C_{test} \end{aligned} \tag{25}$$

where Ω is the (constant) angular velocity in rad/s which is set such that one full revolution is effected in 628 cycles and (x_0, y_0) is the center of the rotation. The initial condition is such that the value in the slotted disk is set to a non-zero value (1.0 here) and outside the disk it is set to zero.

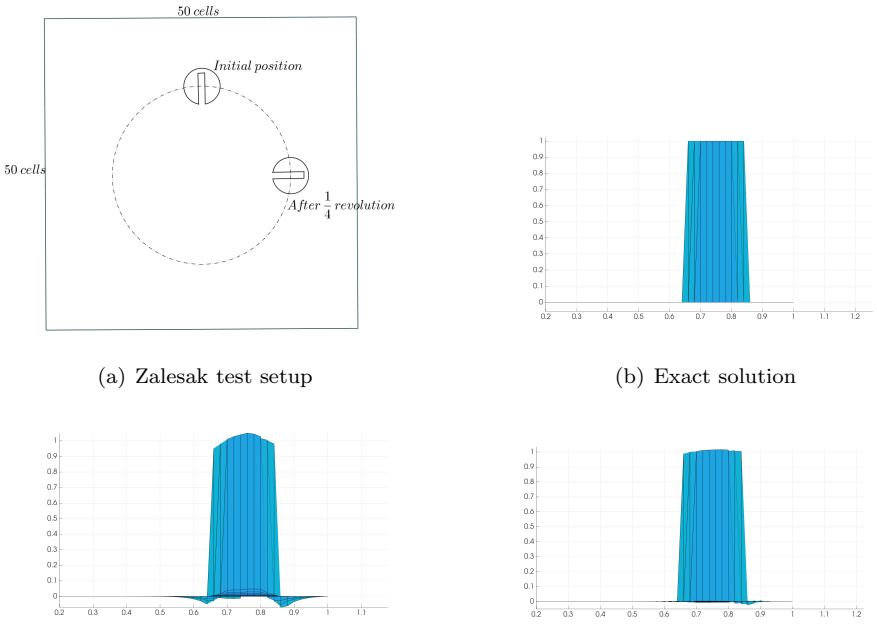

(a) Zalesak test setup

(b) Exact solution

(c) Compact FD

(d) Compact WENO

Figure 4: Zalesak slotted disk test case

Figure 3 shows the comparison between the two schemes for the solution of the Zalesak test case. The compact WENO method reduces oscillations by a large extent compared to the compact FD case. Very little numerical dissipation is added.

5.3. A compressible turbulent jet

The compressible turbulent jet has been simulated as explained in Section 4. The Reynolds number for the tests has been set at a moderately high value of 8500 with a Mach number of 0.9. The tests have been run for two Schmidt numbers, 0.5 and 1.0. The size of the grid is $960 \times 480 \times 480$ with a time step size

of 1/200. The dissipation has been set to low meaning that $\epsilon = 10^{-9}$, $C = 9.0$, $r_c = 0.1$. This ensures that the oscillations are completely damped upto the required level and the solution is still meaningful and not overly dissipated. First, a validation of the compact FD method is shown with experimental results [35, 36] with the help of the normalized averaged centerline velocity. For the purposes of comparison, the Reynolds number and Mach number for this test are 10^4 and 0.5 respectively. Fig 6 shows the decay in the velocity normal to the y direction. Fig 5 shows the effect of the compact WENO method used here and the improvement over the compact FD method and underscores the need for the compact WENO method in this case to accurately capture the discontinuities and remove the oscillations.

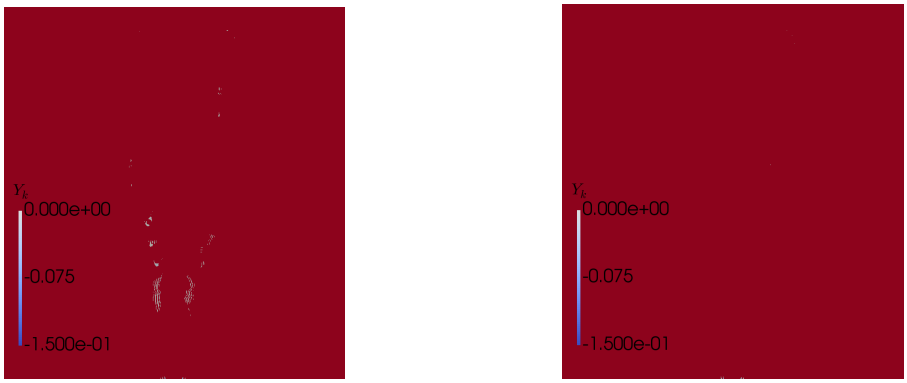

(a) Compact FD (b) Compact WENO

Figure 5: Oscillations in scalar concentration,Y_k fields, Re = 8500

With the compact FD validated, we would like to next show the effectiveness of method in capturing the scalar concentration. The decay rate in the scalar concentration is shown in Fig 7. We see that the expected decay rates are between 5.0 and 5.9 as given in [37]. The decay rates observed here in Table 2 as well in other numerical simulations(eg. [37]) are lower than those of their experimental counterparts. This can be attributed to the disturbances and non-ideal conditions in experiments which are difficult to circumvent/replicate computationally. Fig 8 shows two variations for two different schmidt numbers.

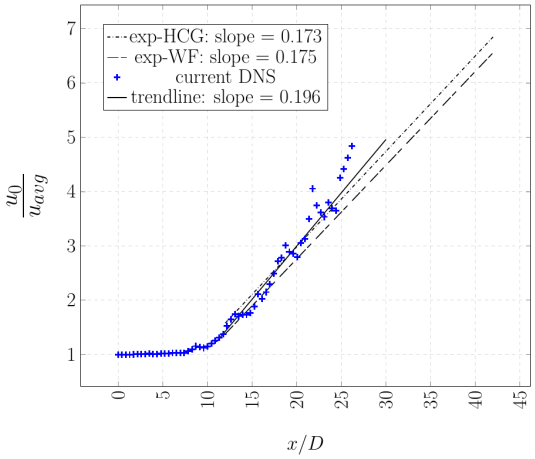

Figure 6: NACV decay at Re = 10^4

We see that for lower schmidt numbers, the dominating instability modes are varicose whereas for the higher Schmidt numbers are helical as expected and even though both the modes can exist, only one mode can dominate the flow [38, 39].

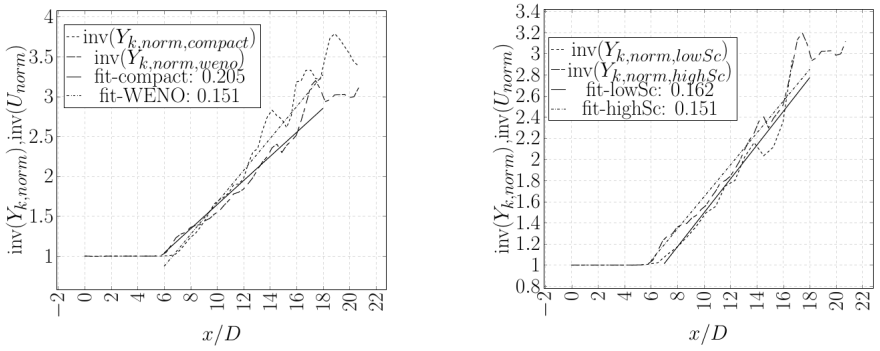

(a) Comparison with compact FD

(b) Comparison of different Schmidt numbers

Figure 7: Decay rate of Y_k at a Reynolds number of 8500.

Method	***Decay rate (inverse of the slopes)***
Velocity, Experimental, HCG [40]	5.78
Velocity, Experimental, WF [40]	5.71
Velocity, Current DNS	5.11
Scalar concentration, Compact FD, Sc = 1.0	4.89
Scalar concentration, Compact WENO, Sc = 1.0	6.62
Scalar concentration, Compact WENO, Sc = 0.5	6.17

Table 2: Decay rates of NACV at Re = 1×10^4

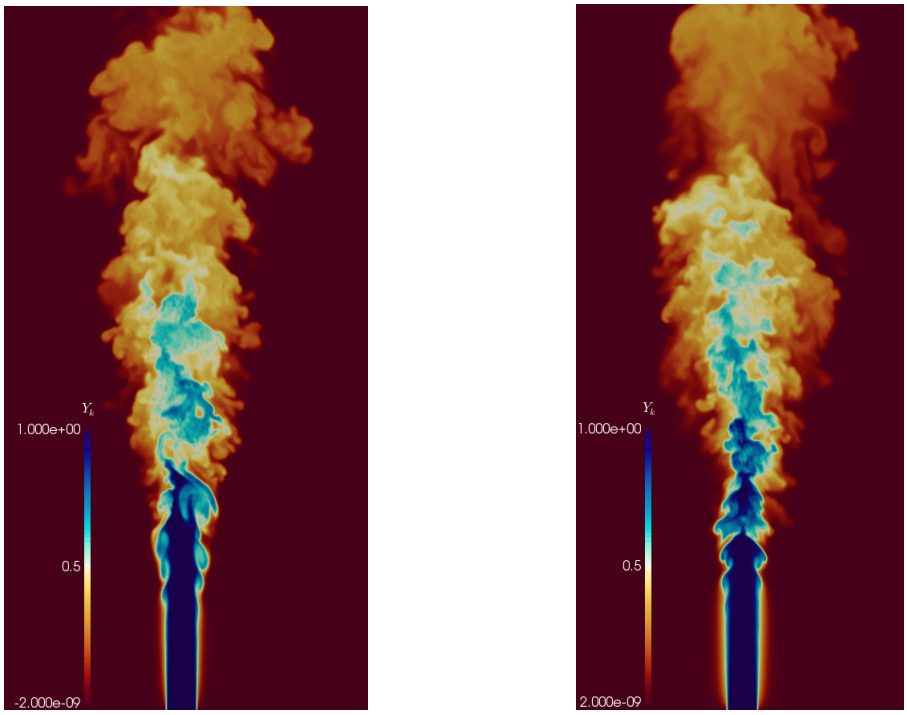

(a) Compact WENO, Sc = 1.0

(b) Compact WENO, Sc = 0.5

Figure 8: Scalar concentration,Y_k fields, Re = 8500

6. Conclusion

In conclusion, we observed that scalar transport in a compressible turbulent jet cannot be accurately modeled by just the compact FD methods. The

staggered compact WENO is a hybrid of the compact FD methods which have been used extensively and the hybrid WENO methods. As the reduction of dissipation is one of the important aspects in WENO and other non-oscillatory methods, a compromise if to use a hybrid stencil, which reduces dissipation while maintaining the non-oscillatory behaviour as developed by Liu et.al. The method has the advantages of stability, high spatial resolution derived from the staggered compact method of Boersma while being able to simulate problems which require a non-oscillatory behaviour. We observed that the dissipation can be controlled as required according to the physical problem at hand. This method is suitable especially for compressible turbulent jets in combustion as they can accurately capture the oxidiation of the fuel and the transport of the scalar species.

References

[1] B. J. Boersma (2005). doi:10.1016/j.jcp.2005.03.004.

[2] X. Liu, S. Zhang, H. Zhang, C. W. Shu (2015). doi:10.1016/j.jcp.2014.12.027.

[3] P. Moin, K. Mahesh (1998). doi:10.1146/annurev.fluid.30.1.539.

[4] S. K. Lele (1992). doi:10.1016/0021-9991(92)90324-R.

[5] K. Mahesh (1998). doi:10.1006/jcph.1998.6022.

[6] B. J. Boersma (2004). doi:10.1016/j.fluiddyn.2004.10.003.

[7] P. Moore, H. Slot, B. J. Boersma (2007). doi:10.1016/j.jcp.2007.04.006.

[8] Y. Shen, G. Zha (2011). doi:10.1016/j.jcp.2011.01.039.

[9] K. K. Q. Zhang, B. Shotorban, W. J. Minkowycz, F. Mashayek (2006). doi:10.1002/fld.1207.

[10] J. Zhao, M. Davison, R. M. Corless (2007). doi:10.1016/j.cam.2006.07.006.

[11] A. Harten, B. Engquist, S. Osher, S. R. Chakravarthy (1987). doi:10.1016/0021-9991(87)90031-3.

[12] C. W. Shu, Journal of Computational Physics 78 (1989) 32–78.

[13] C.-W. Shu, S. Osher (1988). doi:10.1016/0021-9991(89)90222-2.

[14] E. Weinan, C. W. Shu, 1994. doi:10.1006/jcph.1994.1004.

[15] X. Liu, S. Osher, T. Chan, 1994. doi:10.1006/jcph.1994.1187.

[16] G.-S. Jiang, C.-W. Shu 228 (1995).

[17] C. K. W. Tam, J. C. Webb, 1993. doi:10.1006/jcph.1993.1142.

[18] M. P. Martín, E. M. Taylor, M. Wu, V. G. Weirs (2006). doi:10.1016/j.jcp.2006.05.009.

[19] N. Adams, K. Shariff (1996). doi:10.1006/jcph.1996.0156.

[20] Y. X. Ren, M. Liu, H. Zhang (2003). doi:10.1016/j.jcp.2003.07.006.

[21] A. K. Henrick, T. D. Aslam, J. M. Powers (2005). doi:10.1016/j.jcp.2005.01.023.

[22] J. H. Ferziger, M. Peric, 2002. doi:10.1016/S0898-1221(03)90046-0.

[23] F. A. Williams, 1985. doi:10.1137/1.9781611971064.ch3.

[24] N. Peters (2001). doi:10.1088/0957-0233/12/11/708.

[25] S. M. Ghiaasiaan, 2011. doi:10.1017/CBO9780511800603.

[26] C. W. Shu (1998). doi:10.1007/BFb0096351.

[27] S. Pirozzoli (2002). doi:10.1006/jcph.2002.7021.

[28] X. Y. Hu, Q. Wang, N. A. Adams (2010). doi:10.1016/j.jcp.2010.08.019.

[29] D. F. Griffiths, D. J. Higham, 2010. doi:10.1007/978-0-85729-148-6.

[30] J. C. Butcher, 2008. doi:10.1002/9780470753767.

[31] T. J. Poinsot, S. K. Lele (1992). doi:10.1016/0021-9991(92)90046-2.

[32] K. W. Thompson (1990). doi:10.1016/0021-9991(90)90152-Q.

[33] S. Tan, C. Wang, C. W. Shu, J. Ning (2012). doi:10.1016/j.jcp.2011.11.037.

[34] S. T. Zalesak (1979). doi:10.1016/0021-9991(79)90051-2.

[35] I. Wygnanski, H. Fiedler (1969). doi:10.1017/S0022112069000358.

[36] J. Hussein, S. P. Capp, W. K. George (1994). doi:10.1017/S002211209400323X.

[37] D. J. Bodony, S. K. Lele (2005). doi:10.1063/1.2001689.

[38] I. Danaila, B. J. Boersma. doi:10.1016/j.aqpro.2013.07.003.

[39] I. Danaila, J. Dušek, F. Anselmet (1997). doi:10.1063/1.869446.

[40] C. L. Lubbers, G. Brethouwer, B. J. Boersma (2001). doi:10.1016/S0169-5983(00)00026-5.